Nodal gap energy in high-T_c cuprate superconductors: A new paradigm

Hiroaki ANZAI[1,a,*], Masashi ARITA[2], Hirofumi NAMATAME[2], Masaki TANIGUCHI[2], Motoyuki ISHIKADO[3], Kazuhiro FUJITA[4], Shigeyuki ISHIDA[5], Shinichi UCHIDA[6] and Akihiro INO[2]

[1]Graduate School of Engineering, Osaka Prefecture University, Sakai 599-8531, Japan

[2]Hiroshima Synchrotron Radiation Center, Hiroshima University, Higashi-Hiroshima 739-0046, Japan

[3]Comprehensive Research Organization for Science and Society, Tokai, Ibaraki 319-1106, Japan

[4]Department of Physics, Cornell University, Ithaca, New York 14853, USA

[5]Advanced Industrial Science and Technology, Tsukuba, Ibaraki 305-8568, Japan

[6]Department of Physics, University of Tokyo, Tokyo 113-0033, Japan

[a]anzai@ms.osakafu-u.ac.jp

Keywords: High-T_c superconductivity, Angle-resolved photoemission spectroscopy.

Abstract. In high-T_c cuprate superconductors, the *d*-wave-like superconducting gap appears to depart from the standard proportionality with critical temperature T_c, and shows different doping dependences between the nodal and antinodal regions of momentum space. The failure of the attempts so far to formulate these momentum-resolved gaps with T_c has posed questions to their roles in electron pairing and their mutual relationship. Here, we report a simple proportional relation between nodal gap and critical temperature in superconducting $Bi_2Sr_2CaCu_2O_{8+\delta}$ and $Bi_2Sr_{1.6}La_{0.4}CuO_{6+\delta}$. Using low-energy synchrotron radiation on angle-resolved photoemission spectroscopy, we observed the strongly curved gap profile in the underdoped cuprates, and found that a nodal-gap component $2\Delta_N$ at the nodal limit of the gap slope closely follows $8.5k_BT_c$ and concomitantly related to the antinodal-gap energy Δ^* through a reduction factor of square-root superfluid density ρ_s. These empirical formulae provide a new gap-based paradigm on the principle governing T_c in strong-coupling superconductors.

Introduction

In classical Bardeen-Cooper-Schrieffer (BCS) theory, a superconducting critical temperature T_c is proportional to an energy gap in the electronic excitation spectrum [1]. However, this is not the case in underdoped high-T_c cuprates: as hole concentration *p* decreases from the optimum, the amplitude of *d*-wave-like gap Δ^* increases whereas T_c decreases [2,3]. Instead, superfluid density ρ_s decreases along with such underdoping, and thus is considered as a candidate of the superconducting order parameter in the cuprates [4-10]. Recently, a variety of experimental gap energies in the superconducting state have been classified into two groups [11-13]. One increases like Δ^* and the other decreases like T_c with underdoping. The former energy Δ^* remains as a pseudogap above T_c for the underdoped cuprates, as typically seen in the electronic excitation spectra around an antinode [14]. In the close vicinity of a node, by contrast, the gap closes above T_c [15,16]. The further experimental evidences suggest that the low-energy near-nodal excitations are more relevant to T_c than the antinodal ones [16,17]. Nevertheless, the gap energies defined under a dichotomy between near-nodal and antinodal regions have been difficult to formulate along with the doping dependences of T_c and ρ_s [17-19]. The unformulated behaviors of the nodal and antinodal gaps posed severe challenges not only to their mutual relationship but also to their standard role in electron pairing. The identities of these gaps have thus been at the center of controversy over a unified picture of the unconventional pairing state in the high-T_c cuprates, and intensively examined for clues to the principles underlying the peculiar behavior of T_c.

Angle-resolved photoemission spectroscopy (ARPES) is an excellent tool for studying the anisotropic energy gap as it provides direct information of the electronic structure in energy-momentum space. In the previous ARPES studies, two phenomenological fitting models have been suggested to quantify the nodal-gap component from the momentum-resolved gaps $\Delta(\theta)$. One is linear-fit analysis and the other is high-harmonic-fit analysis. The former is based on the presumption that the character of excitation gap discontinuously changes on a certain region of Fermi surface [15,17,18,20,21]. The latter is that the gap variation is described by *d*-wave gap function including the higher harmonic term [22-25], indicating that there is no definable boundary from the node to the antinode. It is debatable whether the near-nodal region is well defined or not. The problem is that it is difficult to determine the nodal gap from only a few *k*-points in the vicinity of the node. Here, we have utilized low photon energies with synchrotron radiation in ARPES measurement. The low-energy photons facilitate improvement in energy and momentum resolution, because in-plane momenta are magnified into large emission angles under a given instrumental angular resolution [15,18,19,21-23,26,27]. Furthermore, the tunability of the photon energy enables us to select the photoelectron final state suitable for the observation of superconducting gap from the node to the antinode [22,23,26,27].

In this paper, we show simple empirical forms,

$$8.5k_{\mathrm{B}}T_c = 2\Delta_{\mathrm{N}} \propto \Delta^* \sqrt{\rho_s}, \tag{1}$$

through a refined ARPES data of bilayer and single-layer cuprate superconductors, $Bi_2Sr_2CaCu_2O_{8+\delta}$ (Bi2212) and $Bi_2Sr_{1.6}La_{0.4}CuO_{6+\delta}$ (Bi2201). Low-energy ARPES provided clear-cut gap images over the entire Fermi surface, and revealed that the gap slope decreases asymptotically toward the node. This observation led us to determine the pure nodal-gap component Δ_{N} from the limit of the gap slope. As a result, the nodal-gap energy Δ_{N} is proportional to T_c, indicating its relevance to the condensation of the electron pairs. A high plateau value of Δ_{N}/T_c ratio exhibits sufficiently strong electron coupling both for Bi2212 and Bi2201. Furthermore, the nodal and antinodal gaps are quantitatively related by a factor of the square-root superfluid density, $\Delta_{\mathrm{N}} / \Delta^* \propto \sqrt{\rho_s}$, in a wide hole-concentration range. This reduction factor is identical to the theoretical prediction for the effect of incoherent pair excitations [28,29], implying that the antinodal gap energy is relevant to the formation of the electron pairs. Thus, we argue that the strong coupling makes a critical difference to the pairing state, and that a substantial number of electrons remain paired, despite dropping out of the coherent superfluid in the underdoped superconducting cuprates. These gap-based formulae reasonably describe a crucial part of the mechanism governing T_c.

Experiment

High-quality single crystals of Bi2212 and Bi2201 were grown by traveling-solvent floating-zone method. Details of sample preparation are described elsewhere [30,31]. Hole concentrations p for Bi2212 have been deduced from the samples' T_c using a phenomenological relation, $T_c/T_c^{max} = 82.6(p\text{-}0.16)^2$, with $T_c^{max} = 91$ K from Ref. 32. Heavily-underdoped and heavily-overdoped samples were made of Dy-substituted and Pb-substituted crystals, respectively. The value of p for Bi2201 was calculated by the form, $p = 0.21 - 0.15x$, where x is the La concentration in this system [33]. ARPES experiments were performed on a helical undulator beamline, BL-9A of the Hiroshima Synchrotron Radiation Center, using a SCIENTA R4000 analyzer. Total instrumental energy resolution was set at 5 meV. Clean surfaces were obtained under ultrahigh vacuum better than 5×10^{-11} Torr. Energies were calibrated with reference to the intermittently monitored Fermi edge of polycrystalline gold.

Results

Figure 1(a) shows intensity plots of ARPES spectra around |ω| = 36 meV for the optimally-doped Bi2212 (T_c = 91 K). We have studied photon-energy dependence of low-energy ARPES, and found that switching the photon energy from $h\nu \leq$ 7eV used in laser-based ARPES studies [15,18,19,21] to 8.5 eV results in a dramatic improvement in the spectral intensity in the off-nodal region. This enabled our high-resolution gap study covering from the node through to the antinode for both the bonding band (BB) and antibonding band (AB) of the CuO_2 bilayer. As typically seen in ARPES spectra of Figs. 1(b)-(d), the superconducting gap gradually opens away from the node, indicating a *d*-wave-like gap structure. The Fermi surfaces were determined rigorously from the minimum-gap loci, because both inaccuracy and broadening of the cutting path result in an overestimate of the gap energy. The spectra along the Fermi surface of BB are displayed in Fig. 1(e) as a function of off-node angle θ (Fig. 1(a)). The seamless evolution of the gap image is obtained from the node to the antinode. Similarly, the gap image for the optimally-doped Bi2201 (T_c = 33 K) has been extracted from the low-energy ARPES data, as shown in Fig. 1(j). The overall reduction of gap energies for Bi2201 in Figs. 1(g)-1(j) explain its lower T_c. The gap size at θ = 22° for Bi2201 is approximately 42% with respect to that for Bi2212, which is consistent with previous results [21].

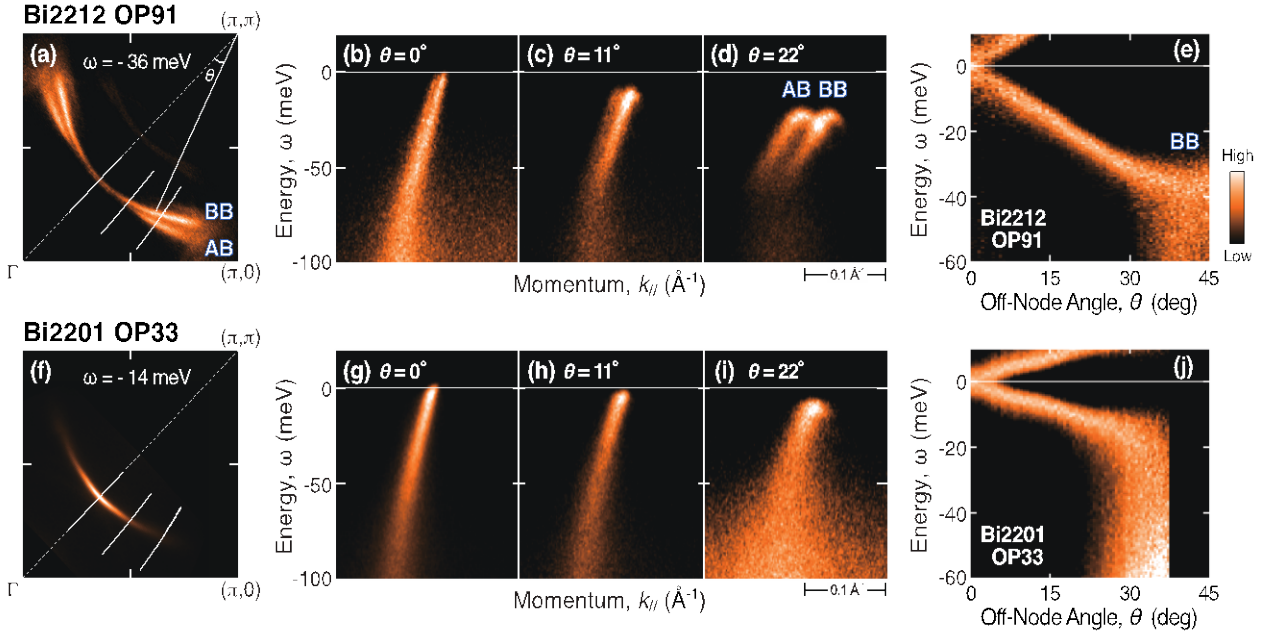

Figure 1 Low-energy synchrotron-radiation ARPES data of optimally-doped Bi2212 and Bi2201. The spectra were measured at T = 10 K with hν = 8.5 eV for Bi2212 (upper panels) and hν = 7.8 eV for Bi2201 (lower panels). (a),(f) Intensity plot of the spectral weight, which is symmetrized with respect to the diagonal of the Brillouin zone. The off-node angle θ is defined about the (π,π) point. (b)-(d) and (g)-(i) ARPES spectra along three typical momentum cuts as indicated white curves in panel (a) and (f), respectively. (e),(f) Energy-versus-θ plots of the spectral images along the Fermi surfaces, which is symmetrized with respect to ω = 0. BB and AB indicate the bonding and antibonding band of CuO_2 bilayer for Bi2212, respectively.

Deviation from the *d*-wave gap is directly imaged in the energy-versus-sin2θ plots of the ARPES spectra. Figures 2(a)-(c) reveal that the curvature of the gap profile in sin2θ < 0.6 increases as hole concentration *p* decreases from the optimum, making clear a departure from the standard *d*-wave form, $\Delta(\theta) \propto \sin 2\theta$, for the underdoped superconducting Bi2212. The superconducting gap energies Δ(θ) were determined by fitting energy-distribution curves (EDCs). For the spectral function A(ω) at

a minimum gap locus, we adopted a widely-used phenomenological form introduced by Norman *et al*. [34],

$$A(\omega) = -\frac{1}{\pi}\mathrm{Im}\left[\frac{1}{\omega + i\Gamma - \Delta^2/\omega}\right], \tag{2}$$

where the peak position and width are given by the superconducting-gap energy Δ and the single-particle scattering rate Γ, respectively. In accordance with the incoherent spectral weight increasing towards higher energies, we added a background linear in energy and then applied the multiplication by a Fermi-Dirac distribution function. As shown in Figs. 2(d)-(c), the EDCs are well captured by this phenomenological function. Here the artifact of the antinodal peak smearing is ruled out of the causes for this deviation [35], because the curvature in sin2θ is established within the region, $|\sin 2\theta| \leq 0.75$, where the well-defined sharp and intense peak is observed for an underdoped sample with T_c = 66 K (UD66), as shown in Figs. 2(b) and (e). We found that the gap slope in sin2θ decreases continuously and asymptotically toward the nodal limit θ → 0 for the underdopd Bi2212. This result indicates that the deviation from the *d*-wave gap penetrates into the close vicinity of the node. So far, it has often been assumed that there is some discontinuity between the nodal and antinodal spectra or a certain region with pure *d*-wave gap [15,17,18,20,21]. However, it is difficult to define them with the all-round seamless images in Fig. 2(a)-(b), because all the spectral features, such as the energy gap, the peak width, the peak intensity, and their derivatives along the Fermi surface, smoothly evolves in going from the node to the antinode. The continuous spectral evolution in momenta has also been reported by Vishik *et al*. [36]. These imply that the nodal region is indefinable from ARPES data for Bi2212. In other words, even near the node, a certain percentage of the antinodal character likely mixes in the spectral behavior. Indeed, the near-nodal gap does not close exactly at T_c [18,19], and the gap-closing temperature gradually decreases to T_c on approaching the nodal limit, θ → 0, in a way similar to the deviation from the *d*-wave gap [15,37].

Therefore, we have adopted the high-harmonic fit over the unbounded region for parameterization of the anisotropic superconducting gap [24,25]. The nodal and antinodal gap energies are defined as $\Delta_N = 0.5(d\Delta/d\theta)|_{\theta=0}$ and $\Delta^* = \Delta(\theta)|_{\theta=45°}$, respectively, so that $\Delta_N/\Delta^* = 1$ is satisfied for the ideal *d*-wave gap as depicted in Fig. 2(c). The fitting function is expressed as

$$\Delta(\theta) = \Delta_N \sin 2\theta + (\Delta^* - \Delta_N)(3\sin 2\theta - \sin 6\theta)/4, \tag{3}$$

where the first term is solely responsible for the nodal-gap slope, the second term models the gap deviation without adjustable angle parameter and its asymptotic behavior is consistent with the empirical indistinctness of the pure *d*-wave region. Note that the onset angle, where the gap deviates from the linearity in sin2θ, is indefinable under this fitting model. Consequently, this function well captures the curved gap profiles Δ(θ) (solid curves) and their nodal tangents $\Delta_N$sin2θ (blue lines) for all the doping levels of Bi2212 and for the optimally-doped Bi2201, as overlaid in Figs. 2(a)-(c) and 3(a). One can find the fact that the nodal limit of the gap slope Δ_N decreases with underdoping from OP91 to UD66, and then to UD42, and seems to follow a similar doping dependence as T_c.

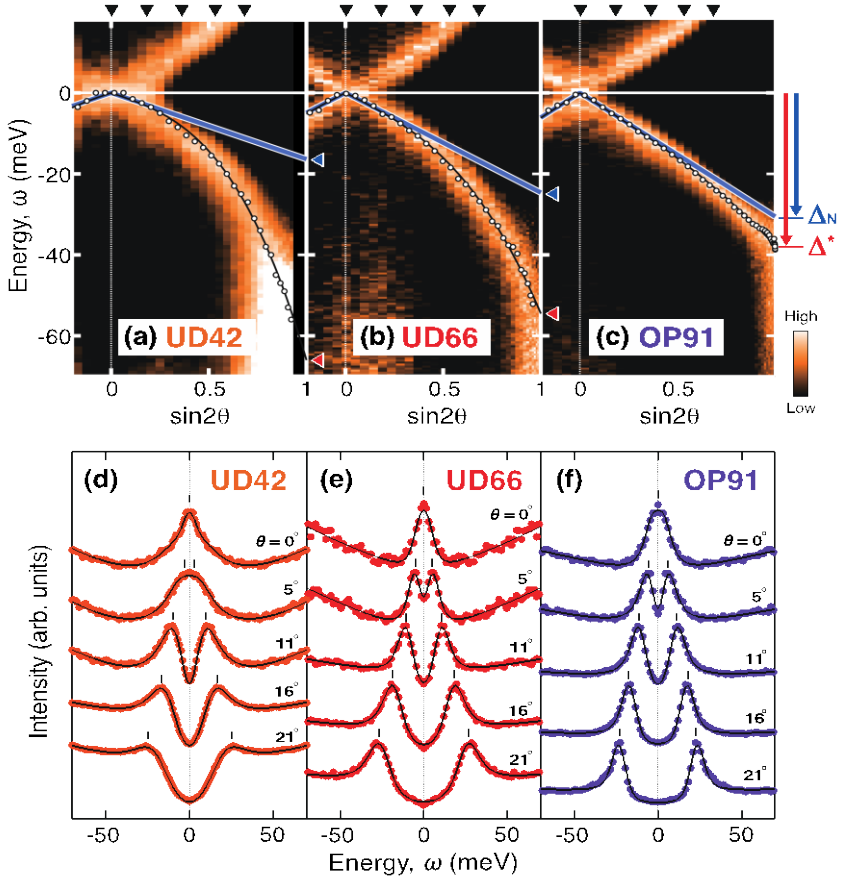

Figure 2 Doping dependence of the gap profiles in Bi2212. Samples are labeled by a doping-level prefix, namely underdoped (UD) and optimum (OP), and a trailing number denoting T_c. (a)-(c) Energy-versus-sin2θ plots of the spectral images for BB, taken in the superconducting state at T = 10 K and symmetrized with respect to ω = 0. Circles, curves and blue lines denote the gap energies, the next-higher-harmonic fits and the nodal tangents, respectively. (d)-(f) EDCs at the momenta marked by black triangles in panels a-c. Black curves and vertical bars denote the fits and the gap energies, respectively. The original data have been reported in Ref. 22.

The gap energies scaled by T_c are plotted in Fig. 3(d), which reveals that the nodal limit of $\Delta(\theta)/T_c$ remains unchanged with underdoping and in different materials in contrast to the antinodal limit. We have determined the two gap parameters, Δ_N and Δ^*, from the high-harmonic fit and plotted as a function of hole concentration in Fig. 3(b). As hole concentration p decreases from the overdoped limit, both the nodal and antinodal ones increase with keeping a constant proportion, $\Delta_N = 0.87\Delta^*$. This is the canonical behavior expected when the coupling is getting stronger. With further decreasing p, the nodal gap $2\Delta_N$ closely follows the decrease in T_c in contrast to the monotonic increases in the antinodal gap Δ^*. The gap-to-T_c ratio is quantified as $2\Delta_N/k_BT_c = 8.5$, which is about twice the mean-field prediction 4.3 for d-wave weak-coupling superconductors. Figure 3(c) shows that our data for Bi2212 and Bi2201 finely converge on the line of $2\Delta_N/k_BT_c = 8.5$ in particular from the optimum to a heavily underdoped level, and that similar values of $2\Delta_N/k_BT_c$ have been reported for other single-layer cuprates [20,21]. It is reasonable that T_c is primarily determined by Δ_N rather than Δ^*, because thermal quasiparticle excitations concentrate in the vicinity of the node and hardly occur around the antinode in particular for the strong-coupling case, $2\Delta^*/k_BT_c >> 4.3$. The association between the nodal excitations and T_c has also been suggested in various experiments [12,13,15-17]. In particular, the decrease in Δ_N with underdoping has been deduced from the low-energy slope of B_{2g}-Raman spectra [12] and the quasiparticle interference in scanning-tunneling images [25].

A new insight arises from the analogy between the doping p and temperature T dependences of Δ_N. With both increasing p and decreasing T, the superconducting gap approaches the ideal d-wave form.

As p decreases conversely, Δ_N is suppressed relative to Δ^*, and expected to decrease towards zero on approaching the disappearance of the superconductivity along $2\Delta_N/k_BT_c = 8.5$. This behavior is quite analogous to what is seen with increasing T (ref. 15). Noting that the superfluid density ρ_s decreases to zero on approaching the critical temperature, $T = T_c$, irrespective of the pseudogap temperature [4,5,7,10], one may associate the nodal-gap suppression, Δ_N/Δ^*, with the low superfluid density ρ_s, which has widely been argued to play a critical role in the underdoped cuprates as the Uemura relation [4,5]. From this viewpoint, we found another simple relation, $\Delta_N / \Delta^* \propto \sqrt{\rho_s}$. Figures 3(e) and 3(f) compare the square of nodal-to-antinodal gap ratio, $(\Delta_N/\Delta^*)^2$, with the superfluid density deduced from the magnetic penetration depth [7,9,10]. The ρ_s for the Bi2212 follows a single doping dependence, which is known as an universal curve for the superfluid density. It increases linearly in hole concentration p with an onset at $p \sim 0.07$, and then shows a saturation at $p \sim 0.19$ (refs 7,10). The intimate relationship between the nodal and antinodal gaps is in accord with the continuity between the nodal and antinodal spectra (Fig. 2(a)-(c)).

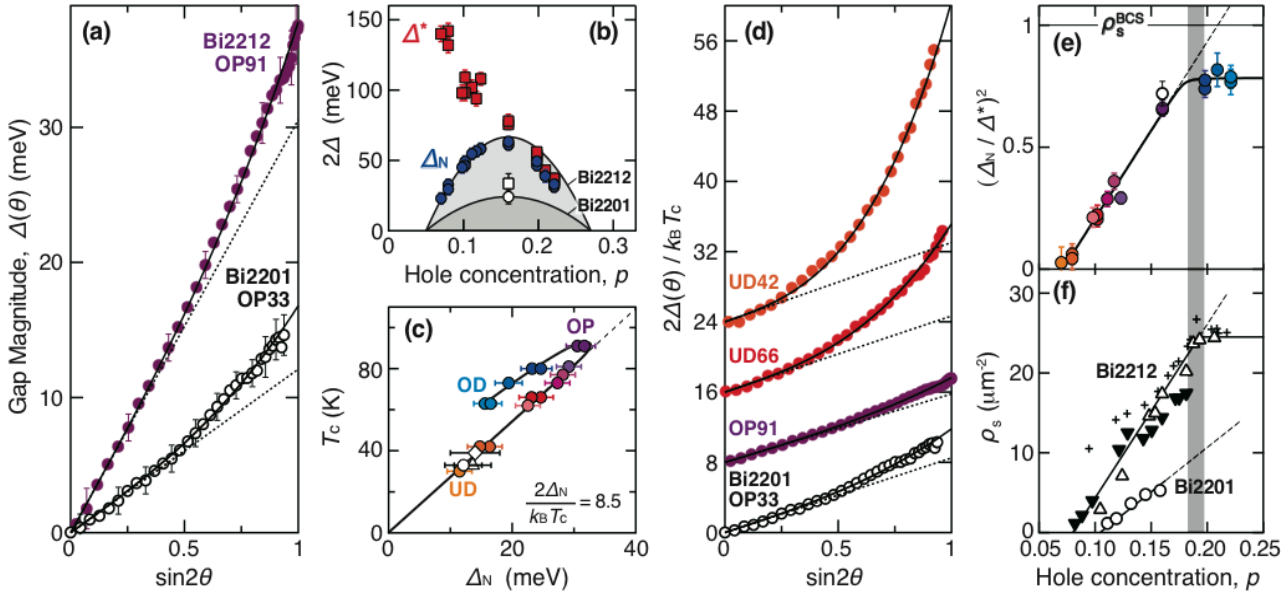

Figure 3 Doping dependence of gap parameters. (a) Gap energies as functions of sin2θ in the superconducting state of optimally-doped Bi2212 (purple circles) and Bi2201 (open circles). (b) Doping dependences of the energies of nodal gap $2\Delta_N$ (circles), antinodal gap Δ^* (squares), and $8.5k_BT_c$ (black curve). Colored and opened symbols are results for Bi2212 and Bi2201, respectively. (c) Correlation between T_c and Δ_N for Bi2212 (colored circles) and Bi2201 (open circle) from the present study. Also plotted are the data for optimally-doped Bi2201 (open triangle) [21] and $La_{2-x}Sr_xCuO_4$ (open diamond) [20]. (d) Superconducting-gap energies scaled by T_c, plotted as functions of sin2θ, and vertically offset by 8 for each sample. Solid curves and dotted lines denote the high-harmonic fits and the nodal tangents, respectively. (e) Doping dependence of square of nodal-to-antinodal gap ratio $(\Delta_N/\Delta^*)^2$. (f) Superfluid density, $\rho_s \equiv \lambda^{-2}$, determined from magnetic penetration depth λ with alternating-current susceptibility (triangles) [10], from heat capacity (crosses) [7] and isothermal reversible magnetizations (circles) [9].

Discussion

A general form of $\Delta_{SC} / \Delta = \sqrt{\rho_s / \rho_s^{BCS}}$ has been theoretically deduced for the superfluid reduction due to the incoherent pair excitations inherent in the strong-coupling superconductors, where the degeneracy between the order parameter Δ_{SC} and the pair-formation energy Δ is split. The former is manifested in the energy of the near-nodal spectral peak as Δ, whereas the latter dominates the

antinodal peak energy Δ^*, as shown by taking into account the lifetime effect [28,29]. In the weak-coupling BCS model, ρ_s^{BCS}, the superfluid density is approximately constant, because the Fermi velocity and Fermi-surface perimeter in the normal state are hardly dependent on the hole concentration p [38]. Therefore, the strong-coupling scenario well explains our empirical form, $\Delta_N / \Delta^* \propto \sqrt{\rho_s}$, with $\rho_s^{BCS} \cong 31$ μm^{-2} and 14 μm^{-2} for Bi2212 and Bi2201, respectively, and is also consistent with the observations of the high gap-to-T_c ratios and the strong renormalization of dispersion upon the superconducting transition [38]. Under this scenario for the nodal-gap suppression, the phase fluctuation persisting down to a temperature below T_c is responsible for the decrease in superfluid density. However, the intrinsic phase fluctuation arising solely from the strong coupling diminishes at temperatures much lower than T_c [28,29]. Hence, in conjunction with the strong coupling, some extra source generating the incoherent pair excitations at low temperatures is assumed to be present, on the basis of the phenomenology among Δ_N, Δ^*, and ρ_s. The possible candidates for this scattering source are the orders competing with the superconductivity [29]. In particular, it has indeed been observed by scanning-tunneling experiments that the nanoscale spatial domains of density-wave-like modulation spread over the underdoped Bi2212 [40]. Perhaps, the limit of $2\Delta_N/k_BT_c \leq 8.5$ may imply that such competing orders are practically inevitable for the strong-coupling superconductivity.

We combin two relations and finally obtain $8.5k_BT_c = 2\Delta_N \propto \Delta^* \sqrt{\rho_s}$. This formulation associates T_c with the superfluid density $\rho_{s\square}$, as well as with the pair-formation energy, $\Delta \cong \Delta^*$ [4,5]. Notably, recent investigations have revealed that the rising exponent of T_c as a power of $\rho_{s\square}$ is generally less than 1, and that specifically $T_c \propto \sqrt{\rho_s}$ is satisfied near ρ_s = 0 [8,9]. This critical scaling can be understood as a narrow-range limit of our form, $T_c \propto \Delta^* \sqrt{\rho_s}$. Empirically, high phase stiffness appears to favor the lowest-order *d*-wave term over the higher-order-harmonics term. Thus, as another possible implication of $\Delta_N / \Delta^* \propto \sqrt{\rho_s}$, the pairing of near-nodal electrons may be dominated more by the requirement of global phase coherence than by the attraction between themselves.

Summary

In conclusion, the ARPES using low-energy synchrotron radiation has revealed the empirical relation among the nodal, antinodal, and critical temperature in Bi2212 and Bi2201. The nodal-gap energy $2\Delta_N$ closely follows with $8.5k_BT_c$ in a wide hole-concentration range and is also proportional to the product of an antinodal gap energy Δ^* and a square-root superfluid density $\sqrt{\rho_s}$, by the form of $8.5k_BT_c = 2\Delta_N \propto \Delta^* \sqrt{\rho_s}$. These relations reveal the nodal and antinodal gaps as representing the condensation and formation energies of electron pairs, respectively, being identical to the formula predicted by a strong-coupling phase-incoherent scenario. Regardless of interpretation, the simple phenomenological formulae put strong constraints on existing theories for the high-T_c superconductivity, and will stimulate broad activities with their potential universality.

Acknowledgement

We thank Z.-X. Shen and A. Fujimori for their useful discussions, and T. Fujita, Y. Nakashima, and K. Ichiki for their help with experimental study. H. Anzai acknowledges financial support from JSPS as a research fellow. This work was supported by KAKENHI (20740199) and Sasakawa Scientific Research Grant (No. 25-202) from The Japan Science Society. The ARPES experiments were performed under the approval of HRSC (Proposal No. 09-A-11, 10-A-24, 12-A-28 and 13-A-20).

References

[1] J. R. Schrieffer, Theory of Superconductivity (Addison-Wesley, New York, 1964).

[2] N. Miyakawa, P. Guptasarma, J. F. Zasadzinski, D. G. Hinks and K. E. Gray, Phys. Rev. Lett. 80, (1998) 157–160.

[3] J. C. Campuzano *et al*., Phys. Rev. Lett. 83, (1999) 3709–3712.

[4] Y. J. Uemura *et al*., Phys. Rev. Lett. 62, (1989) 2317–2320.

[5] V. J. Emery and S. Kivelson, Nature 374, (1995) 434–437.

[6] D. L. Feng *et al*., Science 289, (2000) 277–281.

[7] J. L. Tallon, J. W. Loram, J. R. Cooper, C. Panagopoulos and C. Bernhard, Phys. Rev. B 68, (2003) 180501R.

[8] D. M. Broun *et al*., Phys. Rev. Lett. 99, (2007) 237003.

[9] G. C. Kim, M. Cheon, S. S. Ahn, J. H. Jeong and Y. C. Kim, Europhys. Lett. 82, (2008) 27005.

[10] W. Anukool, S. Barakat, C. Panagopoulos and J. R. Cooper, Phys. Rev. B 80, (2009) 024516.

[11] S. Hüfner, M. A. Hossain, A. Damascelli and G. A. Sawatzky, Rep. Prog. Phys. 71, (2008) 062501.

[12] M. Le Tacon *et al*., Nature Phys. 2, (2006) 537–543.

[13] J. W. Alldredge *et al*., Nature Phys. 4, (2008) 319–326.

[14] A. G. Loeser *et al*., Science 273, (1996) 325–329.

[15] W. S. Lee *et al*., Nature 450, (2007) 81–84.

[16] A. Pushp *et al*., Science 324, (2009) 1689–1693.

[17] K. Tanaka *et al*., Science 314, (2006) 1910–1913.

[18] I. M. Vishik *et al*., Proc. Natl Acad. Sci. USA 109, (2012) 18332–18337.

[19] T. Kondo *et al*., Nature Commun. 6, (2015) 7699.

[20] T. Yoshida *et al*., Phys. Rev. Lett. 103, (2009) 037004.

[21] Y. Okada *et al*., Phys. Rev. B 83, (2011) 104502.

[22] H. Anzai *et al*., Nature Commun. 4, (2013) 1815.

[23] A. Ino *et al*., Nanoscale Research Letters 8, (2013) 515.

[24] J. Mesot, *et al*., Phys. Rev. Lett. 83, (1999) 840–843.

[25] Y. Kohsaka *et al*., Nature 454, (2008) 1072–1078.

[26] T. Yamasaki *et al*., Phys. Rev. B 75, (2007) 140513.

[27] H. Anzai *et al*., Phys. Rev. Lett. 105, (2010) 227002.

[28] Q. Chen, I. Kosztin, J. Boldizsár and K. Levin, Phys. Rev. Lett. 81, (1998) 4708–4711.

[29] C.-C. Chien, Y. He, Q. Chen and K. Levin, Phys. Rev. B 79, (2009) 214527.

[30] H. Hobou *et al*., Phys. Rev. B 79, (2009) 064507.

[31] K. Fujita *et al*., Phys. Rev. Lett. 95, (2005) 097006.

[32] M. R. Presland, J. L. Tallon, R. G. Buckley, R. S. Liu and N. E. Flower, Physica C 176, (1991) 95–105.

[33] Y. Ando *et al*., Phys. Rev. B 61, (2000) 14956R.

[34] M. R. Norman, M. Randeria, H. Ding and J. C. Campuzano, Phys. Rev. B 57, (1998) 11093R.

[35] U. Chatterjee *et al*., Nature Phys. 6, (2010) 99–103.

[36] I. M. Vishik *et al*., Nature Phys. 5, (2009) 718–721.

[37] K. Nakayama *et al*., Phys. Rev. Lett. 102, (2009) 227006.

[38] T. K. Kim *et al*., Phys. Rev. Lett. 91, (2003) 167002.

[39] R. A. Cooper *et al*., Science 323, (2009) 603–607.

[40] K. McElroy *et al*., Phys. Rev. Lett. 94, (2005) 197005.